CHAPTER-2

EXPERIMENTAL DETAILS AND CHARACTERIZATION TECHNIQUES

2.1 Introduction

The present chapter describes the three aspects of the thesis namely material selection, fabrication process, and characterization techniques. The material's selection criteria have been extensively presented in order to select donor polymers, acceptor small molecules, and charge transport oxides as per their processing conditions. Further, the fabrication method of bulk heterojunction organic solar cells is described along with the processing equipment such as spin coating unit, and thermal evaporation system. The establishment of characterization techniques for the OPV devices processed in the ambient condition will be one of our aim in this thesis. Hence, this chapter also describes the brief description of optical, structural, electrical and chemical characterization techniques.

2.2 Experimental details

2.2.1 Materials selection

Organic solar cell performance in terms of both power conversion efficiency and device stability is highly dependent on processing environment and coating methods. Hence appropriate materials selection is required. There are three basic criteria of materials choice in case of organic photovoltaic devices.

(a) High performing donor and acceptor organic semiconductors are required.
(b) Standard organic semiconductor materials for the active layer – There should not be variation from batch to batch production.
(c) The materials should be environmentally stable.

In the quest of high performing donor polymer, homopolymers (eg. P3HT) are recently replaced by the block copolymers with low bandgap and wide absorption spectra. The block copolymers consist of alternate donor (D) and acceptor (A) moieties.[139-142] The strongly coupled vibrations in block copolymers led to high mobility which required for better charge extraction.[143] Moreover the block copolymers degrade faster than homopolymers under accelerated conditions.[144-145] Inspite of having degradation bottleneck, we have selected two D-A copolymers namely, Poly{3,6-dithiophene-2-yl-2,5-di(2-octyldodecyl)-pyrrolo [3,4-c] pyrrole-1,4-dione-alt-naphthalene} (PDPP-TNT)[146] and Poly{4,8-bis[5-(2-ethylhexyl)thiophen-2-yl]benzo[1,2-b:4,5-b']dithiophene-2,6-diyl-alt-3-fluoro-2-[(2ethylhexyl)carbonyl]thieno [3,4-b] thiophene-4,6-diyl} (PTB7-Th)[49] as shown in figure 2.1.

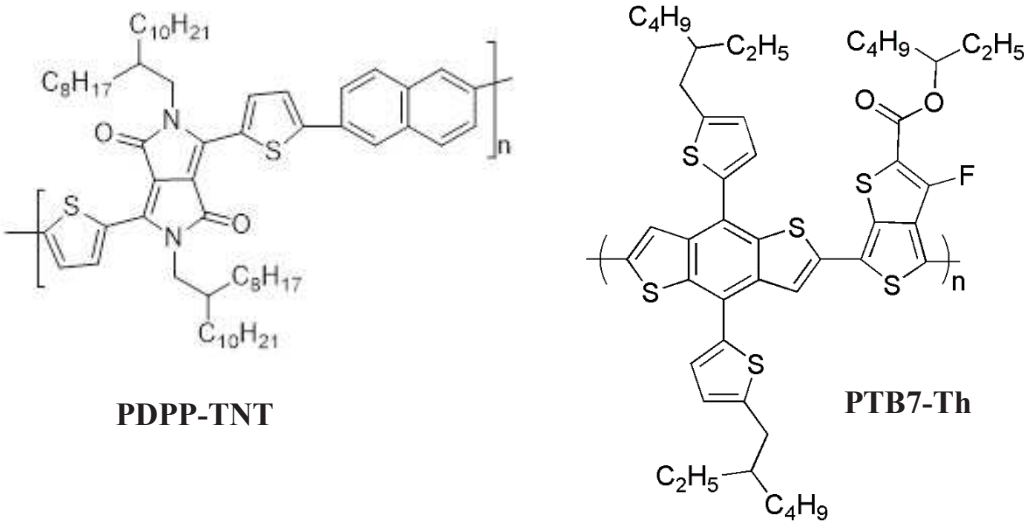

Figure 2.1. The molecular structure of low band gap D-A type copolymers used for OPV devices.

The PDPP-TNT copolymer is having naphthalene and diketopyrrolopyrrole (DPP) as donor and acceptor moieties in the polymer backbone, respectively. PDPP-TNT material was synthesized in-house by *Sonar et al.*[146] and procured from their lab. However, the PTB7-Th block copolymer, a well-established commercial product, was procured from Luminescence Technology Corporation, Taiwan. While 1,8-diiodooctane (DIO), 1,2-dichlorobenzene (ODCB), chloroform, zinc acetate, 2-methoxy ethanol (MEA), Ethanolamine (EA), Diethyl Zinc (DEZ) and molybdenum trioxide (Mo_2O_3) were purchased from Sigma-Aldrich. These chemicals were used as received. We have also purchased pre-cleaned patterned indium tin oxide (ITO) coated glass substrates (Resistivity ~ 15Ω/□), and small molecules such as PC61BM, PC71BM and P3HT polymer from Luminescence Technology Corporation, Taiwan.

2.2.2 Device fabrication

During the course of this work, the inverted configuration of OPV device has been selected for the study as ITO/ZnO/BHJ/MoOx/Ag, shown in figure 2.2. In which two different BHJ active layer will be used for establishment of the material system. The OPV device architecture has various thin film layers and hence diverse processes and techniques are involved in the preparation. These methods will be discussed in the following section. During our studies, we have fabricated and characterized each set of the devices in more than 5 batches and the reproducibility of the data was ensured.

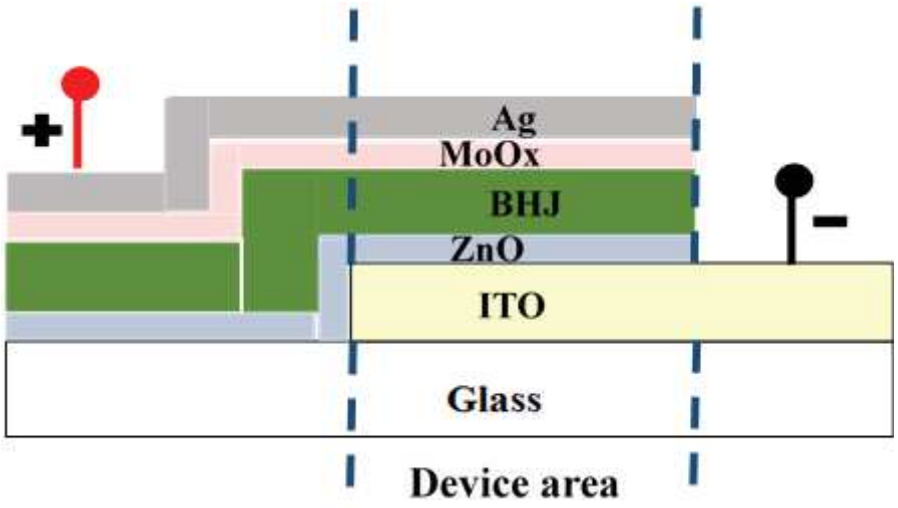

Figure 2.2. Device architecture of inverted BHJ OPV solar cells.

2.2.2.1 Solution preparation

The solution processable OPV devices require blending chemistry with the proper composition in order to get optimized morphology. The ETL and active layer in OPV devices reported in this work are solutions processed. The ZnO as electron transport layer has been derived from zinc acetate (ZnAc) precursor solution. In this case, anhydrous ZnAc, 2-methoxy ethanol (MEA), and ethanolamine were used as received from Sigma Aldrich for making ZnAc precursor solution. A 0.45M ZnAc solution was prepared in a solvent mixture of 96% MEA and 4% ethanolamine.[49] Further, the solution is sonicated for 15 min at 50 ^{0}C temperature and a clear sol-gel is prepared.

The semiconducting donor polymers (PDPP-TNT and PTB7-Th) and acceptor molecule (PC71BM) are received from Lumtec, Taiwan which has been used in making active layer solutions. For making PDPP-TNT:PC71BM solution, the 33 wt.% of PDPP-TNT and 67 wt.% of PC71BM are mixed in a blending solvent of chloroform and o-dichlorobenzene (4:1 by volume).[146] The final concentration of the solution was kept at 15 mg/ml. Thus prepared solution was kept overnight for stirring at hotplate with 50-60 ^{0}C.

However, the PTB7-Th was mixed with PC71BM in 1:1.5 w/w ratio and the solution made in o-dichlorobenzene with overall concentration of 25 mg/ml.[49] The solution was then stirred overnight at 60 ^{0}C temperature.

2.2.2.2 Substrate preparation

Before thin film coatings, the 130 nm thick indium-doped tin oxide (ITO) coated glass substrates were cleaned with previously reported methods. As per that, the ITO substrates were first sonicated for 20 minutes in 2% solution of Micro-90 in de-ionized (DI) water at 50 ^{0}C temperature. Then these substrates rinsed in DI water 3-4 times thoroughly so that soap solution is completely removed. Further, the substrates were sonicated for 20-20 minutes at room temperature in DI water, acetone, and isopropyl alcohol respectively. Drying of substrates has done under Nitrogen flow and activated with UV-Ozone for 25 minutes at 50 ^{0}C temperature.

2.2.2.3 Electron transport (ZnO) and active (D-A BHJ) layer deposition

The prepared sol-gel of ZnAc was filtered with 0.45 μm PVDF membrane and then spin-coated on the pre-cleaned ITO/Glass substrate at 2000 rpm for 60 sec. Further, the substrates were annealed at 250 ^{0}C for 15 minutes to get 40 nm thin film.[97]

The two different spin coating processes have been established for making PDPP-TNT:PC71BM and PTB7-Th:PC71BM BHJ active layers. The PDPP-TNT:PC71BM blend solution was deposited by spin-coating at 5000 rpm for 60 seconds on top of previously coated ZnO layer for making PDPP-TNT based OPV device.[146] The active layer is then annealed on a hot plate at 60 ^{0}C for 10 min to remove the excess solvent. The thickness of the active layer was found ~150 nm. However, the PTB7-Th:PC71BM blend active layer thin film of thickness 90-95 nm prepared by spin coating at 1000 rpm for 90 sec. The Nitrogen environment was used for 30 minutes to dry the deposited thin film without any heating process.

All the solution processes involved in getting ETL and active layers have been done in the ambient condition. The thicknesses of different layers confirmed using DektakXT profiler.

2.2.2.4 Deposition of the hole transport layer (MoO_x) and electrode (Ag)

Further, the hole transport layer (Mo_2O_3) and a metal electrode (Ag) were evaporated in steps onto active layer coated substrates respectively in the thermal evaporation chamber at a pressure lower than 2×10^{-6} mbar. The thickness of these layers was monitored with a quartz microbalance placed near to the substrate holder. The thickness of Mo_2O_3 and Ag was found 10 nm and 100 nm respectively, confirmed using AFM and Dektek thickness profiler.

The devices were then encapsulated with microscopic slide and Delo resin so that they can be studied without a further effect of environment.

2.3 Deposition techniques

2.3.1 Spin coater unit

Spin coating is most commonly used method for applying solution processable thin films. The spin process intermediate steps and the coating unit is shown in figure 2.3. It involves thin film application on the surface of the substrate by uniformly spreading a solution of the required material in a chemical solvent. This process results into a uniform thin film, ranging the thickness from nm to micron. In this process, first, the ink (molecule dissolved in a solvent) spread over the substrate which rotates at high speed. The speed and duration of spinning can be controlled in this system. The solvent is dried due to airflow and plasticized thin film remained. This thin film is either left for some time to get the fully dried film on the substrate or used annealing process.

Spin coating is widely used for organic devices based on organic semiconductors as they require self-assembly and organization during deposition to get a uniform effective thin film. All the key processes happens during the casting and drying stage of an ink as follows[147];

1. Self-assembly of a BHJ active layer
2. Phase segregation of donor and acceptor molecules in BHJ blend
3. Aggregation of nanostrucures

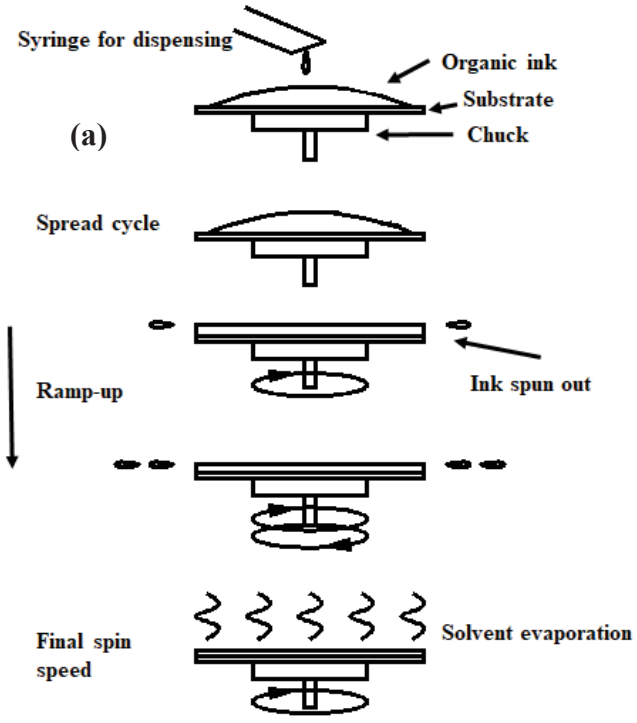

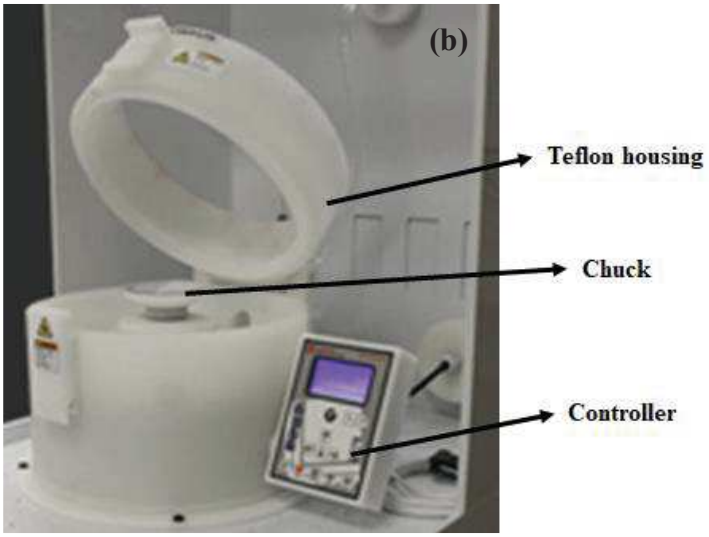

Figure 2.3. (a) Schematic of spin coating steps for thin film deposition. (http://www.physics.uwo.ca/~smittler/images/spincoat.gif), and (b) Image of spin coater.

For most applications, the thickness of the thin film and surface morphology are the crucial parameters. The thickness of the spin-coated film is given by the relation;

$$t \propto \frac{1}{\sqrt{\omega}} \qquad \text{..... (1)}$$

Where t is the thickness of thin film, and ω is the angular velocity of the rotation. However, the exact thickness of the film depends upon the solvent viscosity, temperature, vapour pressure, and humidity. That is why the thickness of the spin coated film of new materials are calculated empirically.

2.3.2 Thermal evaporation system

Thermal evaporator is a physical vapour deposition (PVD) system which is widely used technique to grow highly pure metal and metal oxide thin films with relatively higher deposition rates. This technique involves resistive heating of crucible/boat made of high melting point metals like tungsten, molybdenum, its application is limited only for low melting point material deposition. It can be also used to low melting point small molecule organic materials.

The thermal evaporator deposition chamber has been pumped down by turbo molecular pump backed by the dry rotary pump, but also consists of other accessories like vacuum gauges, material sources, source and substrate shutters, heater cum substrate holder, and quartz

microbalance. Prior the deposition process, the base vacuum inside the chamber must be as high (~ 10^{-6} mbar) as possible to increase the mean free path of evaporated atoms to ensure the good quality of films. The substrates rotated during the deposition of materials inside the chamber in order to maintain the uniform deposition. In thermal evaporation, depositing materials are used in the form of wire, pellets or shots, and is fed onto evaporation boats such as tungsten, molybdenum etc. The materials will be melted in the boat cavity and evaporates as fume from the source and finally, it is deposited on the desired substrates. In this way, a very fine granular microstructure of the evaporated material is found in the deposited thin film. Morphology, environmental stability of the thin film to a large extent depends on the kinetic energy of the atom arriving towards the substrate. Hence the control of deposition rate plays an important role in the thermal evaporation system. The schematic of the system is shown in figure 2.4.

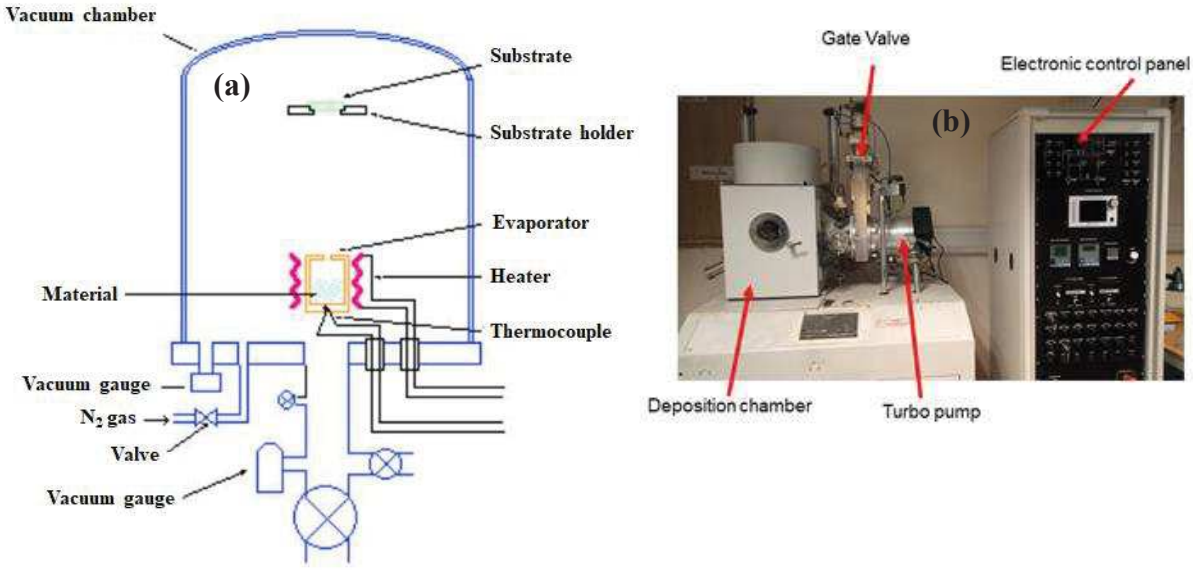

Figure 2.4. (a) Schematic of thermal evaporation unit[148], and (b) Thermal evaporation instrument set-up.

2.4 Characterization Techniques

2.4.1 I-V measurement setup

Keithley 4200 SCS parameter analyzer was used for the current-voltage (I-V) measurements under dark and light. It provides high precision I-V measurement of solar devices. This has an operating voltage of ±10 V with fA current measurements resolution. The illumination source used for light I-V was an AM1.5 Photo Emission Solar Simulator (Model # SS50AAA) with intensity 1000 Wm^{-2}. The light intensity was adjusted with an NREL calibrated Si solar cell. The images of the semiconductor parameter analyzer along with solar simulator is shown in figure 2.5.

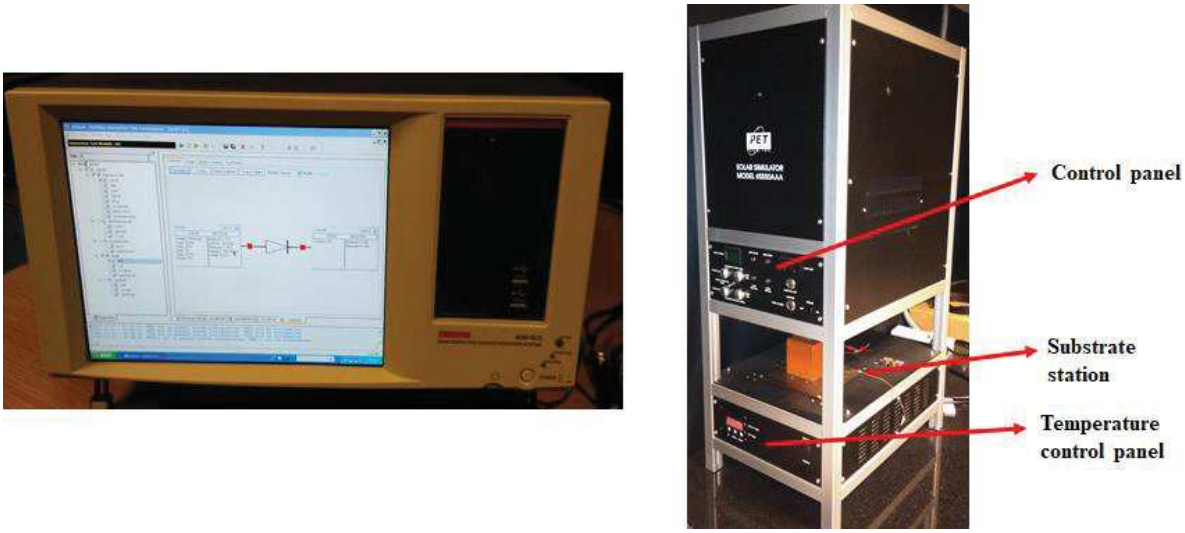

Figure 2.5. (a) Keithley semiconductor parameter analyzer set-up, and (b) Solar simulator.

In the thesis work, primary parameters have been calculated using the I-V measurement of OPV devices under the light. An enhancement of power conversion efficiency (PCE) can be effectively achieved by optimizing the device parameters such as short circuit current (J_{sc}), open circuit voltage (V_{oc}) and the fill-factor (FF) for the intensity of the incident light (P_{in}) as shown in figure 2.6.

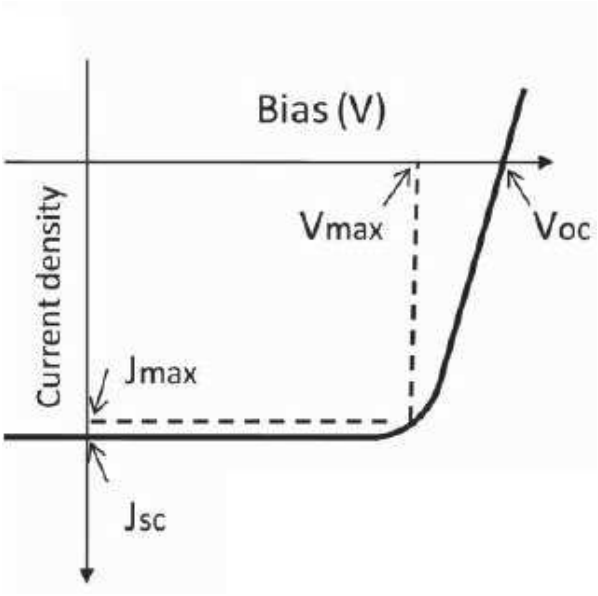

Figure 2.6. Current-density vs bias plot for typical solar cell under light along width basic defining parameters of the device.[149]

The basic equations correlating device parameters are given as;

$$V_{oc} = \left(\frac{HOMO_D - LUMO_A}{q} \right) - 0.3 \quad \text{..... (2)}$$

$$FF = \frac{J_{\max} \times V_{\max}}{J_{sc} \times V_{oc}} \quad \text{..... (3)}$$

$$\eta = \frac{FF \times J_{sc} \times V_{oc}}{P_{in}} \quad \text{..... (4)}$$

2.4.2 Space charge limited current (SCLC) measurement

The space charge limited current method describes the voltage dependence of the current in an insulator or semiconductor sandwiched between the symmetric electrodes. With the help of this technique, the mobility of a single type of charge carrier in organic semiconductors can be calculated with the help of I-V characteristics. By appropriate selection of electrodes, devices are made suitable for the single type of charge carrier conduction. Then charges are injected into the device and when the concentration of injected charge carriers becomes higher than the doped or free charge carriers in the active layer of the device, SCLC region occurs. Mott-Gurney proposed the space charge limited current equation for polymer

diode under some assumptions as (i) active layer should be trap for charge injection, (ii) charge carrier diffusion should be negligible in the active layer, and (iii) electric field at the injecting electric should be zero. Generally, the assumptions (ii) and (iii) remains valid for most of the organic/polymer semiconducting materials.[150] Assuming the trap free semiconductor active layer, the widely acceptable equation was given as;

$$J_{SCLC} = \frac{9}{8}\varepsilon\varepsilon_0\mu\left(\frac{V^2}{L^3}\right) \qquad \ldots\ldots\ldots\ldots\ldots\ldots (5)$$

Where, V is the applied bias across the active layer, L is the thickness of the active layer, μ is the hole or electron mobility, ε is the dielectric constant of the material, and ε_0 is the electrical permittivity in vacuum.

The logarithmic plot between log (J) vs log (V) yields straight line with slope 2. It shows the SCLC region of the semiconducting layer sandwiched between the electrodes as shown in figure 2.7.[150]

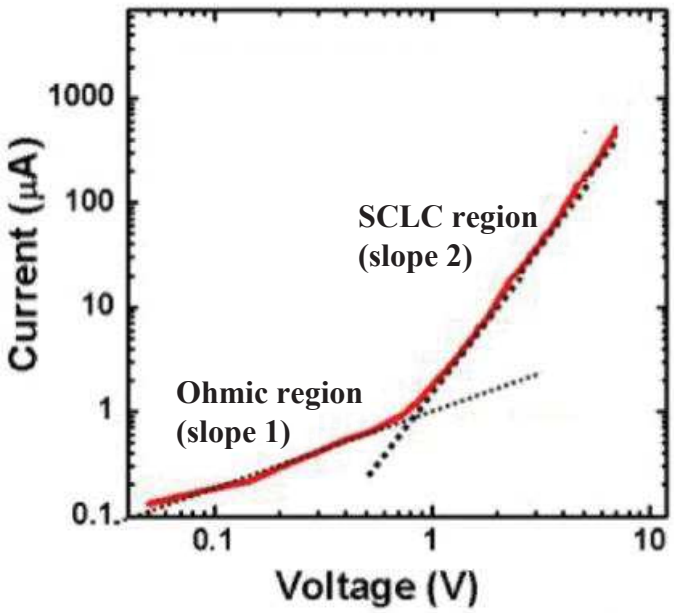

Figure 2.7. SCLC behaviour of polymer semiconductor with Ohmic and SCLC regions.

2.4.3 Incident photon-to-current efficiency (IPCE)

IPCE measurement is the technique to record spectral photocurrent at a particular wavelength and is the very important indicator of a physical phenomenon in solar cells. It can also be used to understand the recombination and diffusion processes in the solar devices. The IPCE is calculated as;

$$IPCE = \frac{\#elctrons_{out}}{\#photons_{in}} = \frac{1240eV.I_{SC}}{\lambda(nm).P_{in}} \quad \ldots\ldots\ldots\ldots (6)$$

Where P_{in} represents the incident light power in Wcm^{-2}, I_{SC} is the short-circuit photocurrent in $\mu A.cm^{-2}$ and $1240/\lambda$ is the incident photon energy in eV at the wavelength λ.

American Society for Testing and Materials Standard has set the standard for the IPCE measurement.[151-152] In this method, the solar cell is kept under working conditions at 1000 Wm^{-2} continuous irradiation. Then IPCE is revealed by scanning the wavelength of chopped monochromatic light in the spectral response range and the photocurrent of the solar cell is measured. The lock-in amplifier is used to separate the total output current from the alternating current output signal. Generally, a chopping frequency of 71-93 Hz is employed considering the balance between stability, noise, and response time of solar cells.[153] This method is suitable for inorganic semiconductor based p-n junction type solar cells, as the response time found about 1 ms.

The response time to solar radiation for the organic semiconductor-based solar cell is found much longer than their inorganic counterparts. In this thesis, the devices were measured for the IPCE using a system from M/s Bunkoukeiki (Model: CEP-25HS-50 SR). The Xe lamp has been used for the illumination of the solar cells and is calibrated using Si-diode.

2.4.4 Impedance spectroscopy

Impedance spectroscopy (IS) is widely used in the field of characterization of materials, and thin films. Recently it has found the application in the investigation of semiconductor interfaces. In impedance method, a small amplitude of alternating current (AC) signal (perturbation) is basically applied to the system with electrical contacts under investigation and the response in terms of current, or voltage, or another signal of interest is measured. The impedance of the system can then be calculated using Ohm's law as;

$$Z(\omega) = \frac{V(\omega)}{I(\omega)} \quad \ldots\ldots\ldots\ldots (7)$$

Where $Z(\omega)$ is the impedance of the system, a complex quantity, which depends on signal angular frequency ω, $V(\omega)$ is the applied AC bias (signal), and $I(\omega)$ is the measured AC current. Therefore, it provides the complete characterization of the resistance, and frequency dependent capacitances and inductances which may act within the device. The frequency dependence can be characterized in terms of the phase shift between current and voltage signals and is

mathematically represented by a complex quantity.[154] The impedance (Z_c) of the ideal capacitor with capacitance C can be given as;

$$Z_c = \frac{1}{j\omega C} \qquad \ldots\ldots\ldots\ldots (8)$$

In this thesis, the organic semiconductor diodes will be measured which have non-linear I-V characteristics and multiple non-radiative recombinations of charge carriers and charge transport in the devices. The frequency dependent physical parameters can be distinguished according to their response to the externally applied AC signal. The impedance analyzer (Autolab PGSTAT-302N) was used for impedance measurements as shown in Fig. 2.8. Impedance spectra were recorded by applying a small voltage perturbation (10 mV RMS) at frequencies ranging from 1 Hz to 1 MHz. The impedance spectrum is called Nyquist plot in which x-axis represents real impedance and the y-axis represents imaginary axis.

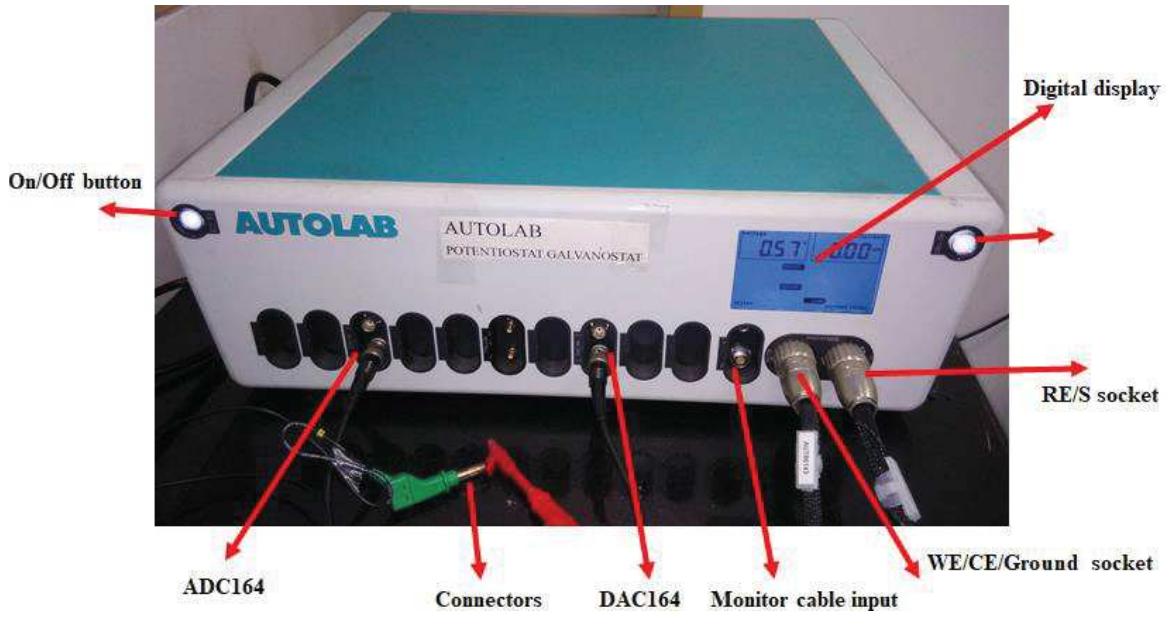

Figure 2.8. Autolab (Model No. PGSTAT-302N) impedance analyzer.

We interpret the measured impedance results by fitting it with theoretical equivalent circuits. There can be a number of equivalent circuits available by which the impedance data matches. Hence the equivalent circuit should have components with appropriate physical meaning in the context of the device under test.

Since the introduction of IS for OSCs by Bisquert[18], several equivalent circuit models have been reported for the fitting of impedance data of OSC devices in the literature. In 2008,

Belmonte *et al.* had proposed an equivalent circuit accounting for the diffusion-recombination mechanism in bulk heterojunction OPV devices.[19] This theoretical circuit model was based on infinite series of parallel RC (resistance-capacitance) circuit as shown in figure 2.9 (a). In which, each electrical parameter was assigned to a particular physical process happening in bulk heterojunction OPV devices such as;

C_n - Stored excess minority carriers gives rise to distributed chemical capacitances.

r_{rec} - Bimolecular recombination of conduction band electrons and valence band holes are modeled by resistive elements.

r_t – Transport of electrons (Transport resistance).

R_s – Series resistance from contact layers and electrodes.

Cg – Device capacitance associated with the depletion region within the active layer.

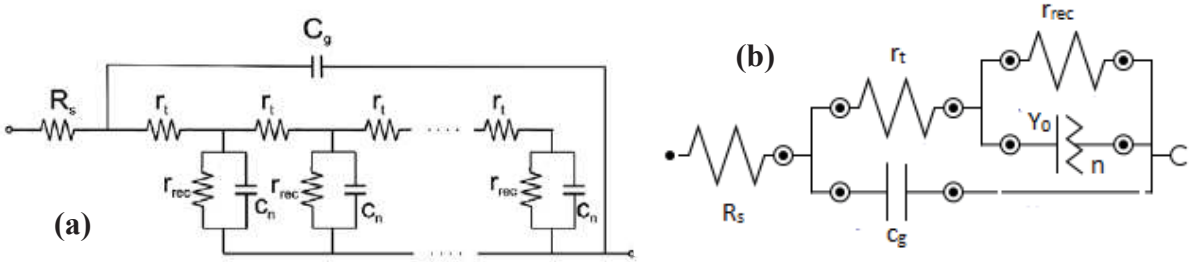

Figure 2.9. (a) Infinite series equivalent circuit model and (b) CPE equivalent circuit model

Though infinite series model was successful in explaining BHJ OPV device physical phenomenon at a certain extent, the tedious fitting calculations had forced to the development of a new model. In 2011, Bisquert et al. have proposed and established a constant phase element (CPE) model to circumvent the need for infinite RC series.[20] The CPE model, shown in figure 2.9 (b), comprised of similar circuit elements except for a CPE element in parallel to recombination resistance and can be explained as;

r_{rec} - Recombination resistance r_{rec} in parallel with a constant phase element.

Y_0 - The coefficient of the CPE.

n - An "ideality" factor characteristic of the distribution of relaxation times.

In this thesis, we have incorporated the well-studied CPE model for the impedance analysis.

2.4.5 Mott Schottky (MS) Analysis

A Schottky contact consists of a metal and a semiconductor surface. The charge carrier concentration (N), present in the semiconductors, affect the electric field distribution at the metal-semiconductor interfaces and hence built-in potential (V_{bi}) found. When the metal and the semiconductor surfaces brought close to each other, charges will move across their interface to provide an equilibrium Fermi level. After this process, there will not be any mobile charges in the semiconductor region near the interface. This region is called charge depletion region and it has a finite width (W). The electrical current flowing across such interfaces is usually non-linear against the bias voltage, as the result of discontinuity of the electronic states responsible for the conduction in the metal and semiconductor materials. The depletion layer width is defined as;[154]

$$W = \sqrt{\frac{2\varepsilon}{qN}\left(V_{bi} - V - \frac{kT}{q}\right)} \qquad \ldots\ldots\ldots\ldots (9)$$

Where, ε is the permittivity of the semiconductor, V is the applied bias, kT/q is the correction factor for majority-carrier distribution tails, N is the charge carrier concentration in the semiconductor, k is the Boltzmann constant, and q is the electronic charge.

In this thesis, we have used the organic semiconductors which are not doped extrinsically. The active layer used is BHJ and it forms a Schottky contact with metal in the OPV device. The Mott-Schottky analysis of the OPV devices will be done using impedance analyzer discussed in the previous section. The devices will be probed for capacitance (C) against varying applied bias at a particular frequency (generally near 1 kHz for organic semiconductors).[154] The Mott-Schottky relation is given as;

$$C^{-2} = \frac{2(V_{bi} - V)}{A^2 q \varepsilon \varepsilon_0 N} \qquad \ldots\ldots\ldots\ldots (10)$$

Where, A is the device area, V is the applied bias, N is the charge carrier concentration, and V_{bi} is the built-in potential. The plot between C^{-2} vs V shows a linear region, which is a good indication of present Schottky contact. The extrapolated extension of linear fit cuts the voltage axis which gives the information of V_{bi}. However, the slope of the linear region gives the charge carrier concentration derived from equation (10) and is given as;[154]

$$N = -\frac{2}{A^2 q \varepsilon \varepsilon_0 \times slope} \qquad \ldots\ldots\ldots\ldots (11)$$

2.4.6 Contact angle measurement setup

Surface wettability of test samples has been investigated by a contact angle (CA) measurement system from Krüss GmbH (model DSA-25) as the one depicted in figure 2.10 in both static and dynamic modes. The CA is commonly defined by the angle where liquid/vapor interface meets the solid surface. In fact, the apparent CA at the liquid/solid interfaces is the outcome of maintaining equilibrium condition at the respective free energies between solid, liquid and vapor.[155]

The main component of CA system includes high performing dosing system, a stage for sample positing, tilting and controlling temperature, camera, and related software for precise CA analysis. In this system, software-controlled pendant drop mode is used where 2 μL droplets of deionized water were dropped onto the sample surface by a needle. A high-speed CCD camera equipped with a magnifying lens was used for capturing the droplet images, and confirm the repeatability of the recorded data at different positions on each sample. In order to measure CA under various gaseous atmosphere, an environment chamber was employed to cover the sample stage. The error in the measured CA was found to be within ± 1.

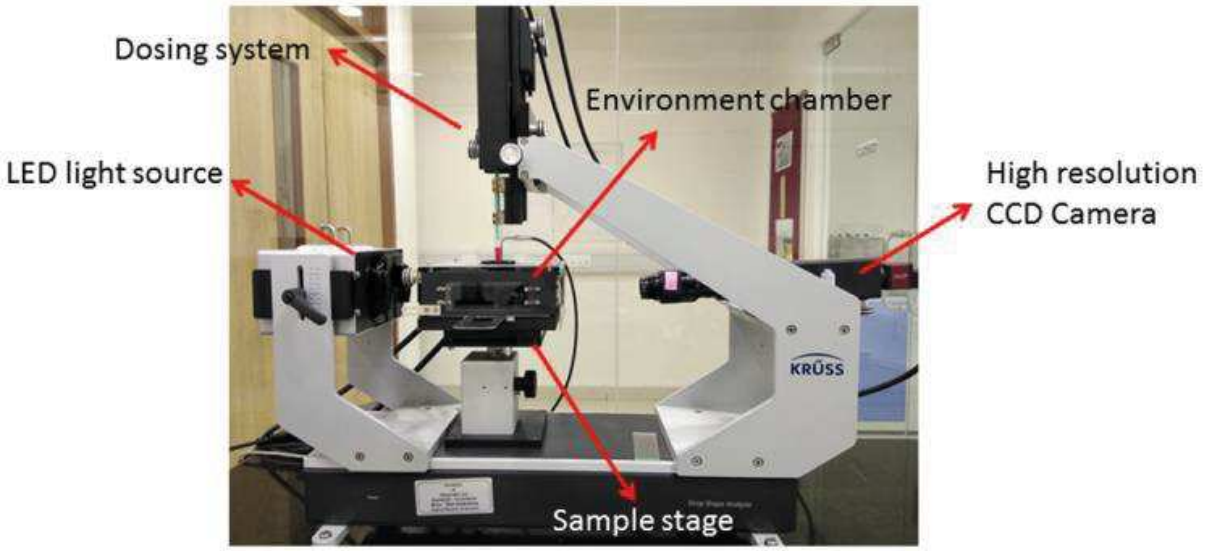

Figure 2.10. Photograph of contact angle measurement setup (Kruss, DSA25) with all accessories.

2.4.7 Atomic force microscopy (AFM)

Local surface morphology on the sample surfaces have been examined by atomic force microscopy (AFM) from Park (XE-7), where the concept is based on near-field interaction of the probe tip with atoms of the investigating surface. The image of this system is given in figure

2.11. This can be achieved by focusing a laser beam on the top surface of the cantilever, while the reflected light is detected by a position sensitive photodiode (PSPD). The sample surface is scanned by the probe tip, and during the scanning the atomic force between them lead to bending of the cantilever. This can be monitored by reflecting laser beam sensed through photodiode and eventually send this signal to the detector. This signal is further converted to image via image processing. Here, the distance between the tip and sample surface is precisely maintained through an electronic interface which supplies the voltage for controlling the piezoelectric scanner by feedback control system.[156] According to the distance between the tip and sample surface, the modes of operation are separated into four major groups[157-158]:

a. Non-contact mode: In non-contact mode, it works in attractive force regime between tip and the sample surface. During the scan, a large tip to sample surface distance is maintained. Due to this the non-contact mode offers faster scan rate which eventually results in poor resolution because of comparatively weak atomic interaction with the atoms of cantilever tip.

b. Contact mode: In this mode, data acquisition occurs at repulsive force region between the tip and sample surface. Here the cantilever is always in contact with the sample surface and therefore the resolution is very high owing to very large atomic forces at the cost of low scan rate.

c. Tapping mode: This is most widely used mode and work at intermediate force region between the attractive and repulsive forces. This is also known as intermittent contact mode. In this mode, the tip oscillates with a set frequency and amplitude, and brings the tip in contact of the surface to acquire high resolution image. Then it lifts the tip off to avoid the surface damage.[156] The reduction of the oscillation amplitude from the set amplitude state is used to measure surface features. The advantage of tapping mode over other modes is that it provides phase imaging. By mapping phase images, it can detect several properties such as composition, adhesion, friction and also viscoelasticity. The imaging carried out in the thesis work was executed using tapping mode.

d. Lateral force mode: Lateral force microscopy which is also known as friction force microscopy is variation of static contact mode. When the tip moves in the lateral direction on the sample surface, the friction force between tip and the surface generates lateral force on the cantilever which induces a torsion on the cantilever. The degree of this torsion is eventually detected and converted to image signal. This mode is used very specific purpose to calculate the surface friction.[156]

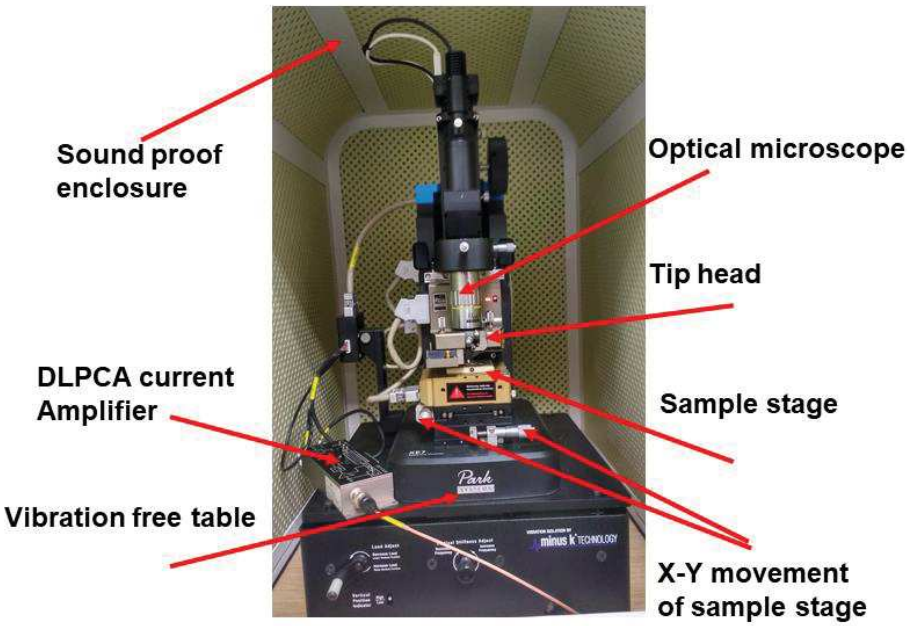

Figure 2.11 Image of Park XE-7 system.

The atomic force microscopy offers large range application apart from only imaging or phase detection. In fact, Park XE7 system is integrated with many other characterizations such as conducting AFM (c-AFM), scanning kelvin probe microscopy (SKPM), magnetic force microscopy (MFM), etc. In this thesis, we have calculated the work function of the modified surface via SKPM. SKPM is a non-contact technique to map the two-dimensional contact potential difference (V_{CPD}) between tip and sample surface at nanoscale resolution. The measured V_{CPD} can be converted to corresponding work function of the sample using the following standard equation,[159]

$$W_{sample} = W_{tip} - qV_{CPD} \quad \text{..... (12)}$$

Where, W_{sample} and W_{tip} are the work functions of the investigating sample and the tip respectively.

2.4.8 Ultraviolet-Visible spectroscopy

The basic working principle is based on the measurement of light absorption due to electronic transitions in a sample under probe. It is generally termed as UV-Vis spectroscopy because the light wavelength required for electronic transitions is typically in the UV and visible region of the radiation spectrum. Optical absorption is a fundamental property of all the materials and it determines the optical properties of materials such as photoluminescence, photovoltaic, and photocatalytic properties.[160] When the incident light interacts with the sample

surface, some photons are transmitted from the surface, some are scattered and rest are absorbed. The absorption of light by an optical sample is quantified as absorption coefficient (α).[161] It is defined as the fraction of incident power absorbed by a unit length of the medium and is correlated with the intensity of light given by Beer-Lambert's law;

$$I(t) = I_0 e^{-\alpha t} \quad \text{..... (13)}$$

Where, I(t) is the intensity of the light transmitted through the sample of thickness t, and I_0 is the incident intensity of the light.

The Tauc had proposed an empirical relation for the determination of optical band gap of semiconductors as;[162]

$$\alpha h\upsilon = A(h\upsilon - E_g)^n \quad \text{..... (14)}$$

Where, α is the absorption coefficient, E_g is the optical band gap, A is a constant related to the type of electronic transition, and here, n could be 1/2 (allowed direct transitions), 2 (allowed indirect transitions), 3/2 (forbidden direct transitions), and 3 (indirect transitions). By extrapolation of linear plot between $(\alpha h\nu)^n$ vs hν, one can determine the band gap of the sample material.[162]

We have used absorption spectra mode of ultraviolet-visible (UV-Vis) spectroscopy for the investigation of the thin film samples made of glass or quartz. For the measurement of absorption spectrum, the transmitted light across the sample surface is recorded by the detector at each incident wavelength to get the desired information. The photograph of UV–Vis spectrophotometer (Shimadzu SolidSpec-3700) is shown in figure 2.12.

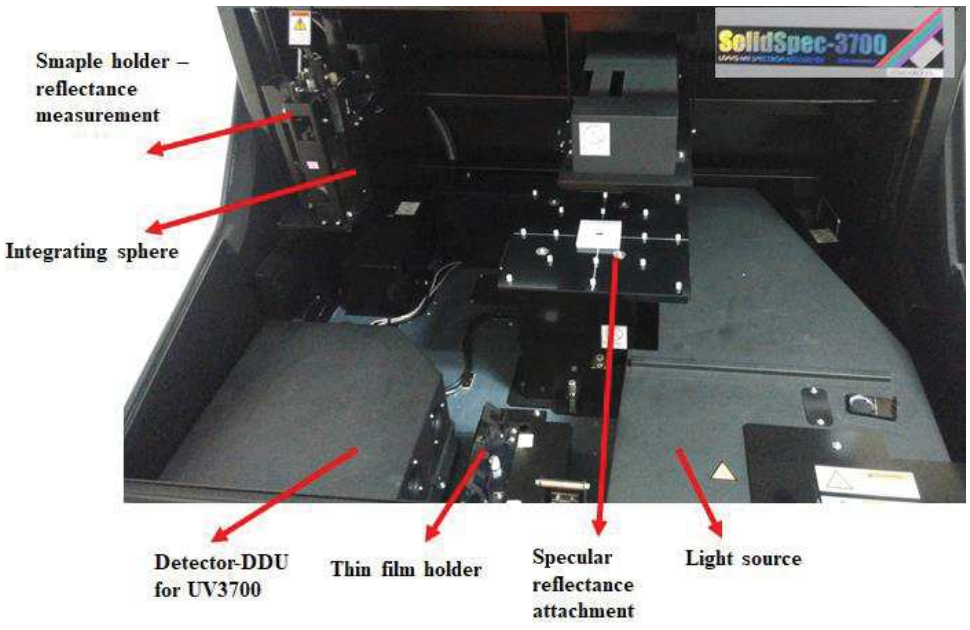

Figure 2.12. Major components of UV-Vis spectrophotometer (SolidSpec-3700) instrument.

2.4.9 Glancing angle X-Ray diffraction and X-ray reflectivity

The grazing incidence X-ray diffraction (GIXRD) technique is used to study the crystal orientation of thin films. In the present study, crystallinity of as-grown and ion beam irradiated films were identified by GIXRD using a Cu-K_α radiation ($\lambda = 0.154$ nm) at an incidence angle of 0.5^0 and over a 2θ scan range of 20^0-80^0, where θ is the Bragg angle. The photograph of X-ray diffractometer (Bruker, D8-Discover) along with its different components is shown in figure 2.13.

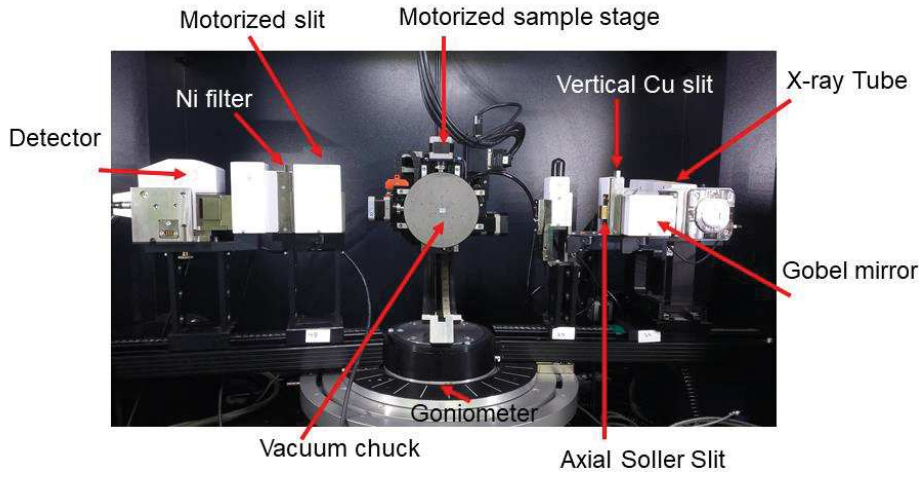

Figure 2.13. Image of glancing angle X-ray diffractometer (Bruker, D8-Discover).

The tungsten filament in X-ray source generates electrons by thermionic emission. The emitted electrons are then accelerated towards the Cu target with an applied high voltage of 40 kV across the X-ray tube. The maximum energy of lab-scale X-ray source is around 8.5 keV. The X-rays are then guided by a soller slit to fall on the sample surface. Cu target emits two X-rays i.e. Cu K_α and K_β. The diffracted K_β are filtered using Ni filter in detector side. In addition, another soller slit is placed before the Ni filter with their slits perpendicular to the one in the source side. The diffracted data are then collected by 1D LYNXEYE XE detector. The acquired data are then analyzed using JCPDS data.

On the other hand, X-ray reflectivity (XRR) which is a powerful characterization technique to investigate film thickness, surface roughness and corresponding electron density of the film, has been used in a systematic way in the same instrument. The reflectivity data was recorded by maintaining equal incident angle (α_i) and exit angle (α_f), and by keeping the horizontal scattering angle to zero. The scattered X-rays are detected with the same 1D detector (LYNXEYE XE) with varying α_i. At this specular condition ($\alpha_i = \alpha_f$), the perpendicular

component of the momentum transfer vector (q_z) provides structural information of the sample. The data were then fitted by Parratt's algorithm to extract ρ as a function of depth (z).[163] The electron density (ρ) of the film can be calculated using the following equation which is a function of refractive index (n), scattering amplitude per electron (r_0), and wave vector (K= 2π/λ),[164]

$$\rho = \frac{\delta K^2}{2\pi r_0} \qquad \text{…….. (15)}$$

A MATLAB program was used to fit the reflectivity data and extract the required parameters.

For this thesis work, the XRR measurements were carried out at the reflectivity beamline BL-4 at INDUS 1, Indore, India with the wavelength of 80 Å. Reflectivity beamline is comprised of a grazing incidence Toroidal Grating Monochromator (TGM) and toroidal mirrors for pre- and post- focusing optics. The beamline is designed to cover 40 – 1000 Å photon wavelength range. Further, the details of the beamline are given in the report by Nandedkar *et al*.[165] The experimental station in this beamline is a high vacuum reflectometer, comprised of the t-2t goniometer and a z-translation stage to keep the sample in and out of direct beam[166]. A silicon XUV photodiode is used to measure reflected beam intensity.

2.4.10 X-ray photoelectron spectroscopy (XPS)

X-ray photoelectron spectroscopy (XPS) is a surface sensitive technique which analyzes the elements constituting the sample surface, its composition, and chemical bonding states by exposing x-rays on the sample surface, and measuring the kinetic energy of the photoelectrons emitted from the surface of the sample.[167] We have used the XPS instrument using ESCA+ (Electron Spectroscopy for Chemical Analysis) equipped with monochromatic Aluminium source (Al kα radiation hv =1486.7ev) from omicron nanotechnology, Oxford Instrument Germany. It can generally acquire information on elements within a few nanometers of the sample surface. XPS instrument and its schematic used for this thesis work is shown in the figure 2.14. The main parts of the XPS system, used for the chemical analysis, are the high vacuum chamber (base pressure of 10^{-10} Torr), X-ray source, hemispherical electron energy analyzer and detector.

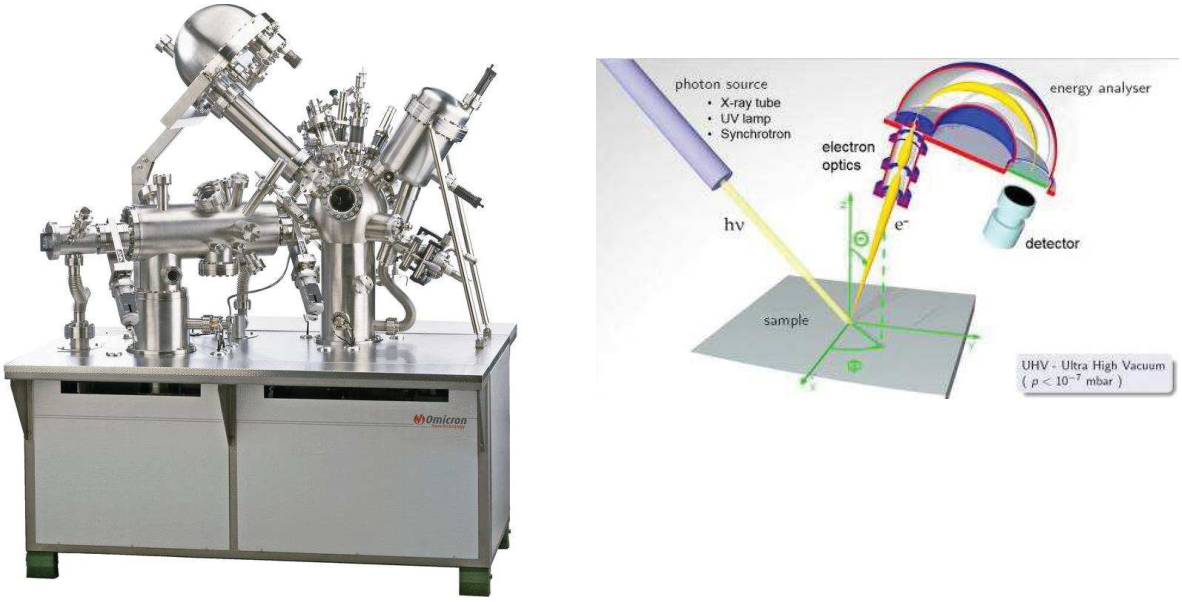

Figure 2.14. Photograph of X-ray photoelectron spectroscopy system along with schematic diagram.

XPS is based on the photoelectric effect where incident photon is absorbed by an atom in solid, leading to the excitation of electronic states (called ionization) followed by the emission of core/inner shell electrons from the surface. The kinetic energy (E_K) of ejected photoelectron depends upon the energy of incident photon (hν) and electron binding energy (E_b) given by the following relation[167-168];

$$E_K = h\upsilon - E_b - \phi \qquad \text{..... (16)}$$

Where, ϕ is the material work function, hυ is the energy of incident photon. The ejected photoelectrons are guided to the hemispherical analyzer with the help of a lens system, and finally filtered and collected by a detector according to their E_K.

The instrument was operated at 15 kV and 20 mA for our work in this thesis. Samples were investigated by Al-Kα source of XPS system integrated with a hemispherical analyzer of radius ~124 mm. To overcome the charging problem a charge neutralizer of 2 keV is applied and binding energy of C1s core (284.6ev) was taken as reference. Resolution was confirmed to 0.60 eV by FWHM. Calibration of E_b scale was made using the gold Fermi edge.